1.0 Key Findings

1.1 *Influence of cement composition*

The influence of cement composition on changes in engineering properties under sodium sulfate attack was investigated by monitoring expansion of Portland cement mortar bars and by measuring compressive strength of Portland cement paste cubes prepared from Type I and V cement [see refs. 1 or 2 for a review of the sulfate attack process]. The interpretation of this data is aided by microCT and EDXRD. All samples considered in this section were produced with *w/c* of 0.485.

Average mortar bar expansion values until an exposure time of 52 weeks are shown in Figure 1. After an apparent latent period extending approximately 13 weeks into the exposure, the Type I bars expanded more rapidly as compared to the Type V samples. At 52 weeks of exposure, the average expansions for Type I bars were 2.09 %, while the Type V bar average expansion was 0.45 %. In general, the standard deviations increased with time for the Type I bars, but such behavior with time was less apparent in the Type V bars. This increase in standard deviation with exposure may result from the inhomogeneities (e.g., cracking, spalling) induced in the samples during sulfate exposure leading to increased variations in the measurements among the different mortar bars of the same type.

In general, the expansion associated with sulfate attack is believed to largely result from the formation of ettringite due to the reaction of ingressing sulfate with existing hydration products (i.e., monosulfoaluminate hydrates, calcium aluminate hydrates) and with residual, unreacted phases (i.e., tricalcium aluminate or C_3A and tetracalcium aluminoferrite or C_4AF). The formation of gypsum, from the reaction of ingressing sulfates with calcium hydroxide, may produce some expansion, but the formation of ettringite is viewed as the more predominant cause (see [3], for example). The composition differences between the Type I and Type V cement and the resulting variations in types and relative amounts of hydration products are likely responsible for the differences in mortar bar expansion measured with continuing exposure.

First, the greater C_3A content in the Type I cement as compared to the Type V cement (9.85% vs. 3.25%) will influence the relative amounts of ettringite and monosulfate initially formed on hydration, and hence the propensity for later expansion by ettringite formation upon sulfate exposure. In addition, any unhydrated C_3A remaining may also result in ettringite formation and expansion, although EDXRD did not indicate the presence of any unhydrated C_3A in our samples.

Secondly, the potential effect of the greater relative amount of C_4AF in the Type V cement as compared to the Type I cement (11.1% vs. 8.2%) needs to be considered. Due to the greater quantity of C_4AF, ettringite formed in Type V cement samples during sulfate attack is likely to be Fe-substituted. Iron-substituted ettringite is believed to be non-expansive or less expansive [17,18]. Thus, the lower C_3A content and the likelihood of ettringite being Fe-substituted are factors that may have contributed to the lower expansion observed in the Type V mortar bars.

Thirdly, the lower ratio of tricalcium silicate to dicalcium silicate (i.e., C_3S/C_2S) of the Type V cement is also likely contributing to its superior sulfate resistance as measured by expansion and changes in strength with exposure (discussed next). The ratio for Type V cement was 2.24 as compared to 10.81 for the Type I cement. There is evidence that sulfate-induced damage is linked, in some cases, to cements with higher C_3S content [4,19].

Average compressive strength measured for Types I and V cement pastes up to 24 weeks of exposure are shown in Figure 2. For comparison, average 14-day compressive strengths for control samples (i.e., samples retained in saturated limewater bath for 2 weeks beyond the initial 3-days curing) were 7000 psi and 5850 psi for the Type I and V cement pastes, respectively. Until 8 weeks of sulfate exposure, the average compressive strengths increased for both the Type I and Type V cement paste samples, as compared to the average compressive strengths after 2 weeks of exposure. The increase in average compressive strength until 8 weeks of exposure for both Types I and V cement samples may be expected due to the continued hydration of the samples in the sulfate solutions [11] and pore filling by the reaction products of sulfate attack [20]. However, by 17 weeks of exposure, the average compressive strength of the Type I cement samples had decreased to 4940 psi, while in the Type V cement samples continued to increase to 7500 psi. By 24 weeks, the strength of the Type I samples further decreased to

2680 psi, and the first decrease in strength for the Type V samples was noticed (f_c = 6750 psi). These results show clearly the superior resistance of the Type V cement in terms of retention of compressive strength during sulfate exposure.

MicroCT was used to track the evolution of physical damage in corresponding Types I and V cement paste cylinders exposed to sodium sulfate solution. Figures 3 (a-c) and 4 (a-c) show three-dimensional reconstructions of the top half of Type I and V specimens, respectively, after 17, 42 and 52 weeks exposure. These reconstructions of the Type I sample show that edge cracking (cracks near the sample edge) (Fig. 3 a), was followed by body cracking (Fig. 3 b) and spalling (Fig. 3 c). Reconstructions of the Type V sample show no physical manifestations of damage at 17 weeks (Fig. 4 a), but after 42 and 52 weeks exposure some cracking at the sample edge is apparent (Fig. 4 b and c). Physical damage was first observed at 17 weeks in the Type I sample as compared to the Type V sample, where cracking at the edges was first observed after 26 weeks of sulfate exposure. Body cracking was first evident during microCT imaging at 36 weeks for the Type I sample, but was not apparent until 52 weeks in the Type V sample. Also, spalling at the sample edges was first observed at 42 weeks of exposure in the Type I cement paste sample, but has not been observed in the Type V cement paste sample after 78 weeks of exposure. Thus, in addition to the earlier appearance of these forms of damage in the Type I sample, the rate of damage progression was more rapid for the Type I cement paste sample.

Spatially resolved EDXRD data has been collected for both controls (i.e., samples stored in air-tight containers after the initial curing period) and sulfate-exposed samples (i.e., samples exposed to sulfate solution after the initial curing period). Figure 5 shows, for Type I and Type V cements, the relative amounts of ettringite and monosulfate hydrate as a function of depth and exposure time in the samples before sulfate exposure and after 52 weeks in sodium sulfate solution.[1] Monosulfate hydrate was observed as the 12-water form ($Ca_4Al_2O_6(SO_4)\cdot 12H_2O$ or "12-water monosulfate") and/or 14-water form ($Ca_4Al_2O_6(SO_4)\cdot 14H_2O$ or "14-water monosulfate"). In Fig. 5(a), all the curves for ettringite are on the same relative scale as one another, enabling a quantitative comparison between different exposure times and cement types, assuming that any variation in ettringite composition between the samples leads to minimal variation in the structure factor of the diffraction peak used to generate this data. Due to experimental limitations, the relative scales for the ettringite and 12-water and 14-water monosulfate hydrate are not the same, and quantitative comparisons describing the relative amounts of the phases in relation to one another cannot be made. That is, quantitative comparisons can only be made when examining the same phase in different samples, *not* when comparing different phases within the same or different samples.

As expected due to the higher C_3A content of the Type I cement, the Type I control contains more ettringite and monosulfate than the Type V control. Very little monosulfate is detected in the Type V cement control, as would be expected [21-23]. In the Type I control both the 12 and 14-water forms of monosulfate are detected; it is well-known that these monosulfate phases can react during sulfate attack to form ettringite (see, for example, [3]). After 52 weeks of exposure, however, the maximum amount of ettringite observed in both the Type I and Type V samples is remarkably similar, which was not expected based on data in the literature [24]. As there was much less monosulfate in the Type V control than the Type I control, with no observation of unhydrated C_3A, and no obvious corresponding depletion of C_4AF, the data suggests that aluminum for ettringite formation in the Type V sample might be coming from a source other than monosulfate and residual unhydrated phases. Gollop and Taylor [21-23] report the close admixture of Al^{3+} in calcium silicate hydrate (C-S-H), and it seems possible that this is a potential source of Al^{3+} for continued ettringite formation in the absence of observable depletion of crystalline Al-bearing phases.

The ettringite curves for the Type I and V cement pastes after 52 weeks sulfate exposure (Fig.5(a)) show marked differences when comparing the relative amounts of ettringite detected near the sample

[1] Crystalline Na-bearing phases are not observed in either the Type I or Type V samples. This observation is consistent with the previous observation that very little Na can be detected in Na_2SO_4 attacked pastes beyond the near-surface region (Gollop and Taylor, 1992).

surface (~0-1.5mm) and at greater depths (~2.5-3.5mm) in each sample. The ettringite concentration varies much more with depth in the Type I sample than in the Type V sample. This observation, which is also true for the ettringite depth profiles of Type I and V samples subject to other sulfate exposure durations, is perhaps consistent with a somewhat different mechanism for the formation of ettringite in the two samples. If the ettringite formed in these samples leads to expansion, the much stronger variation of ettringite concentration as a function of depth in the Type I sample when compared to the Type V sample, likely leads to different stress states in the two types of samples.

In Figure 6(a), EDXRD composition-depth profiles for a Type I cement paste control sample are presented. Crystalline phases typically resulting from cement hydration, including ettringite, monosulfate, and calcium hydroxide, are identified throughout the 4-mm depth interrogated. Ettringite is present in greater quantity near the surface of the specimen, in a region where there appears to be a corresponding decrease in the amount of 12-water monosulfate, relative to that observed at greater depths. The data for calcium hydroxide perhaps indicates that some very near-surface depletion has occurred. The considerable point-to-point fluctuations in the $Ca(OH)_2$ data are due to the relatively large size of those crystals compared to the volume sampled in the EDXRD experiment. In addition, there was evidence for unhydrated C_4AF throughout the depth examined; this data has not been included to simplify the data presentation in this figure.

The corresponding composition profiles for a Type I specimen after 52 weeks of sodium sulfate exposure are shown in Fig. 6(b). Both the monosulfate phases are further depleted in the near-surface region, relative to observations of these phases in the control sample (Fig. 6(a)). In the region where the monosulfate is depleted (first ~1.5 mm), the amount of ettringite is much greater than found in the control, clearly suggesting the well-known progressive reaction of monosulfate to form ettringite as sulfate diffuses into the sample. After 52 weeks of sulfate exposure the near surface region is clearly depleted in calcium hydroxide to a depth of over 0.5 mm. It is notable that *no gypsum* is detected in the Type I sample at 52 weeks of sulfate exposure.

In Figure 7(a), composition depth profiles for a Type V control sample are presented. As in the Type I control sample (Fig. 6(a)), crystalline products of hydration, including ettringite, monosulfate (here, detected as 14-water monosulfate only), and calcium hydroxide, as well as some unhydrated C_4AF, present throughout the sample depth, are detected. As with the Type I control sample, the amount of ettringite near the sample surface is greater relative to the interior of the sample.

Figure 7(b) presents the corresponding profiles for a Type V paste sample after 52 weeks of exposure to sodium sulfate solution. No 12-water monosulfate hydrate is detected in this sample, and the small amount (see Fig 5(b) for comparison with other samples) of 14-water monosulfate present appears to be concentrated near the surface in a region that is substantially free of calcium hydroxide. One remarkable feature of this data is the near-surface depletion of calcium hydroxide, which occurs to a much greater depth than was observed in the 52-week Type I specimen. This difference is possibly related to the lower C_3S/C_2S in the Type V cement, which would then result in less calcium hydroxide initially produced by cement hydration as compared to the Type I and is likely also related to the consumption of $Ca(OH)_2$ in chemical reactions with the ingressing sulfates to form, for example, gypsum and ettringite. Thus, it is also notable that in the near-surface region a band of gypsum is observed at ~ 1mm below the surface. The curves for gypsum and ettringite in this region are clearly anticorrelated in this sample; similar behavior was also observed for other Type V specimens with different sulfate exposure times and with different sulfate solution concentrations [25]. Previously, it has been suggested that gypsum, rather than ettringite, forms when SO_4^{2-} is available, but the available Al^{3+} has been consumed [3]. However, the anticorrelation between gypsum and ettringite seen in the present data does not agree with this. It is possible that some of the ettringite originally present in the 52 week sample at 0.7-1.5 mm depth decomposed to form gypsum and perhaps other products which were either non-crystalline or not detectable for other reasons. The decomposition of expansive ettringite into gypsum, if accompanied by strain recovery, could change the local stress state and lead to cracking.

There is literature [7,26,27] indicating that the decomposition of ettringite to gypsum may be related to a decrease in pH and in all our specimens, gypsum was only observed in regions that were substantially free from calcium hydroxide. Although $Ca(OH)_2$ has been depleted in the 1.4mm nearest the surface for our 52-week Type V sample the detection of ettringite very near to the sample surface (Fig. 7(b)) gives evidence that the pH remains high enough for ettringite stability in this region. This suggests that either the pH profile between the sample surface and the region still containing $Ca(OH)_2$ is complex or that the anticorrelation between the ettringite and gypsum curves is not driven by pH. Another possible explanation is that the ettringite partly converts to gypsum due to high local sulfate concentrations. This behavior has been predicted in a study examining the stability of ettringite in alkaline environments as a function of pH and sulfate ion concentration [28]. Also, sodium ions suppress the solubility of $Ca(OH)_2$ and increase the solubility of gypsum. This influence on pH of pore solution needs also to be examined.

The anticorrelation between the gypsum and ettringite profiles could also be interpreted as an indication of gypsum crystals depositing into preexisting cracks in the cement paste. The microCT data has sometimes shown cracks parallel to the sample surface (i.e., "ring" and/or "longitudinal" cracking) at the depth where EDXRD shows that the first gypsum band begins. That is, the presence of gypsum seems to be sometimes associated with ring or longitudinal cracking. For example, in Figure 10 a crack is observed at 64 weeks at a depth of ~0.9 cm, which closely matches the location of a band of gypsum at 52 weeks (Fig. 8). However, comparison of microCT slices and 3D renderings with corresponding EDXRD data for the same volume of cement paste does not fully corroborate this theory of gypsum product formation within cracks. Specifically, gypsum has been observed in samples *prior* to the observation of a crack; also, gypsum is seen in samples displaying no obvious cracking by microCT; and, finally, the location of the gypsum band locations migrate inward with time (see Fig. 8, discussed next). Each of these observations suggests that cracks may not be required for gypsum formation. However, the limitations of the techniques used must also be considered: it is possible that radial cracks too small to be discernible by microtomography may exist [21-23], and with EDXRD, the thickness of a gypsum band can be reliably estimated only if it lies nearly parallel to the sample surface. While it can be difficult to distinguish if the gypsum is forming within a crack (when one is observed) or in the adjacent paste, the cracks that are observed seem to be of insufficient thickness to accommodate deposits of gypsum of the thicknesses suggested by the EDXRD. Thus, cracking followed by gypsum crystallization in the cracks does not seem fully consistent with the data. Rather, it appears as though much of the gypsum exists or forms in the paste near the crack, when cracks are present.

In general, the pattern of gypsum formation has varied with cement type in the samples examined. As briefly mentioned previously, EDXRD data from Type V samples show that the gypsum-bearing zone migrates inwards over time (Fig. 8) and that the total amount of gypsum in the sample increases with time. In marked contrast, in Type I samples exposed to the same sulfate-attack conditions, the gypsum layer makes only a transient appearance. A relatively small amount of gypsum forms at a depth of ~0.5 mm below the surface after 10 weeks, but at 36 weeks very little remains, and no inward migration has taken place (Fig. 9). Surprisingly, after 42 weeks exposure or more, no gypsum was observed in the Type I samples. The behavior of both sample types suggests that once gypsum has been deposited it can later re-dissolve or react to form other products. However, in the case of the Type V samples as the gypsum in the near surface region is depleted more gypsum is formed at greater depths, but in the Type I samples no new gypsum crystallites are deposited at greater depths. Further research is clearly necessary to better understand the role of gypsum in sulfate deterioration.

2.2 *Influence of w/c*

Concrete and cement paste with lower w/c has been shown to possess greater resistance to sulfate attack (see [1-4], for example). Previously, microCT characterization of pastes at *w/c* of 0.45, 0.50, and 0.60 showed that the onset of sulfate damage (in 10,000 ppm sulfate in Na_sSO_4 solution) was more rapid

at higher w/c [14]. As a result of this understanding, various agencies (e.g., ACI, CEMBUREAU, etc.) make recommendations regarding maximum w/c for anticipated exposure conditions, as well as other requirements for cement composition, use of supplementary cementitious materials, and strength. As the severity of the sulfate exposure condition increases, the recommended maximum w/c in concrete decreases. Here, the influence of w/c was investigated by examining expansion of Type I Portland cement mortar bars and comparing these results with the damage to cylindrical Type I Portland cement paste samples, as measured by microCT. Two w/c were examined – 0.485 and 0.435.

In the present study, expansion of Portland cement mortar bars under sodium sulfate attack was greater for higher *w/c* (Fig. 11), which is in line with the expected behavior for concrete. Until about 12 weeks of exposure, average expansions were similar in both cases. Beyond this period, the average length change increased more rapidly for the samples with the higher *w/c*. Average expansion at 52 weeks was much greater for the higher *w/c* samples, as expected.

When comparing expansion data in Figures 1 and 11, it is notable that a decrease in *w/c* from 0.485 to 0.435 (with Type I cement) and the substitution of Type V cement (with *w/c* of 0.485) for Type I both produce similar decreases in mortar bar expansion, as compared to Type I bars with *w/c* of 0.485. However, the initial latent period when very little expansion was observed, was much shorter for the Type V cement samples (about 13 weeks) than for the Type I lower *w/c* samples (27 weeks). This similarity in performance shows that there exists some flexibility in the design of economical Portland cement mortar mixtures resistant to sulfate attack. The disparity in the latent period also shows the need for longer monitoring of expansion samples to gauge performance.

MicroCT was used to image the physical manifestations of damage in cylindrical cement paste samples at w/c of 0.485 and 0.435. While the expansion data generally agrees with expected behavior with changing *w/c*, the physical damage observed in cylindrical cement paste samples by microCT was more severe at the *lower* w/c. This result was unexpected.

Volumetric reconstructions of a Type I cement paste sample at *w/c* of 0.485 and exposed to sodium sulfate solution for 17, 42, and 52 weeks have been shown in Figure 3 and were discussed in Section 3.1. Observations of the same 2-D slice over time allow the evolution of damage in a sample to be tracked. Slight variations of tilt in the sample within the microCT 40 sample holder produced slight variations in the closest matching slices; thus, pre-existing voids in the sample were used as fiducials to establish matching slices in the samples over time. Figure 12 (a-d) shows the matching slices, where fiducial voids or pores have been labeled P1-P5, at 21, 36, 42, and 52 weeks of exposure for the same sample. At this position near the end of the sample, no damage was observed at 21 weeks (Fig. 12(a)). At 36 weeks (Fig. 12(b)), a surface radial crack (RC1) has just begun to form; some body cracks in the middle of the slice are also present. In Figure 12 (c) the body cracks are barely visible (in fact in this data set, 42 weeks exposure, the main portions of the cracks lie slightly above the plane of the slice); and in Figure 12 (d), 52 weeks exposure, solid body displacement of the central core relative to the outer shell (i.e., along the cylinder's axis) has brought the body cracks farther from the slice shown. At 42 weeks of exposure (Fig. 12(c)), the width of RC1 has widened to 0.16 mm; spalling was observed and a ring crack (C1) had a width of 0.26 mm. At 52 weeks of exposure (Fig. 12(d)), the width of RC1 has grown to 0.22 mm; some spalling continues, and the width of C1 measures 0.68 mm.

Near the ring crack C1 at 42 weeks (Fig. 12(c)) and 52 weeks (Fig. 12(d)), a very dense region (i.e., lighter pixels) was observed at the crack surfaces. The very dense region at the crack surfaces had a linear attenuation coefficient of about 2.4 cm^{-1} at 42 and 52 weeks of exposure, which is greater than the 1.6 to 2.2 cm^{-1} measured elsewhere in the sample. The linear attenuation coefficients were measured as an average of five values near the position shown. The exact underlying cause for the formation of the very dense region at the crack surfaces is not clear, but it is likely that reaction products are forming in this region due to reaction with the ingressing sulfate solution.

Immediately adjacent to this dense region toward the sample core, a less dense region (darker in color), as compared to the sample core, was observed. The linear attenuation coefficient of the less dense region adjoining C1 was 1.3 cm^{-1} and the thickness of this region was 0.7 mm at 42 weeks of exposure;

for the same less dense region at 52 weeks of exposure, linear attenuation coefficient was 1.5 cm^{-1} and thickness was 0.8 mm. The less dense region adjoining the crack is believed to be due to leaching of calcium hydroxide, decalcification of C-S-H, or some other dissolution process resulting from exposure to the external solution at the cracked surfaces.

Figure 13 shows volumetric renderings at 9, 16, 22 and 32 weeks of exposure for the same Type I Portland cement sample at the lower w/c of 0.435. At 9 weeks, the first physical manifestation of damage edges – cracking at the edges – was observed. It is notable that the first physical manifestations of damage are apparent earlier, at 9 weeks vs. 17 weeks (for the w/c of 0.485), in the lower w/c sample. By 16 weeks of exposure, damage had progressed significantly: existing cracks have widened and new cracks have formed (Body cracks were first apparent at 13 weeks). MicroCT at 22 weeks of exposure shows continued crack growth and the first observation of longitudinal cracks along the sample surface (not visible in the image shown). At 32 weeks, cracking and spalling were more extensive than at earlier times. The low w/c cement paste samples completely disintegrated after 56 weeks of exposure. Interestingly, each of the samples of this type subjected to this exposure broke at approximately mid-height, with relatively flat fracture surfaces (Fig. 14). At the sample ends, expansion and cracking can be noted. This flat fracture surface with the observation of cracking and expansion in the sample seems to suggest the development of tensile stress along the long axis of the sample, leading to brittle, localized failure. (For comparison, an entirely different pattern of cracking is noticed for the 0.485 w/c samples, Figure 15, which remain largely intact, but heavily cracked, at 108 weeks. The presence of multiple cracks, running longitudinally and radially, in the higher w/c samples suggests a more multiaxial state of stress.)

The earlier appearance of damage and the more rapid failure (i.e., disintegration) of the lower w/c cement paste warrants further discussion. The potential effects of reduced workability, degree of hydration, changes in extensibility, and pore structure were considered. As described in detail by Naik [25], analysis of the microtomography data showed only a small difference in void volume fraction (0.4% air at w/c of 0.485 vs. 2% at 0.435) between the samples prior to exposure, indicating that variations in workability likely had no major role in the unexpected behavior of the cement paste samples at the lower w/c. The potential influence of a greater amount of unhydrated or residual C_3A at lower w/c was also considered. However, as no residual C_3A was detected by EDXRD in the samples at any age, the role of unhydrated C_3A is likely minor, if contributing at all.

Rather, it is proposed that changes in extensibility and pore structure are more likely factors resulting in earlier cracking in failure in the lower w/c cement paste samples. As w/c decreases, the compressive strength and elastic modulus of concrete or cement paste increases [29]. In such materials, the tensile strength may also be higher than in normal strength concrete or paste, but the relative increase in tensile strength does not scale with the relative gains in compressive strength and stiffness (i.e., gains in tensile strength are quite small, relative to increases in compressive strength and E as the w/c decreases.) This reduces the extensibility (i.e. ability to deform without cracking) of material. That is, for a given tensile elastic strain, with increasing stiffness, the tensile stress induced will increase. Thus, given that the extensibility would be decreased as w/c decreases, it might be expected that cracking would occur earlier in those samples, as was observed here. The observation of flat fracture surfaces at the lower w/c (Fig. 14) – a pattern which is indicative of tensile failure in brittle samples - substantiates the likelihood of the role of decreased extensibility in these samples.

Changes in the pore structure with decreasing w/c should also be considered. With a reduction in w/c, the microstructure of hardened cement paste is refined and pore sizes generally decrease. Measurements of linear attenuation during x-ray microtomograpny have suggested that the voids in the pastes become filled with material during sulfate attack [15,25]. Scherer [30] has considered damage resulting in brittle materials by crystallization in pores. Among other factors, Scherer reports that greater stresses are developed when crystallization occurs in pores of smaller size. Hence, reductions in w/c, while improving impermeability, may produce a microstructure *in cement paste* (i.e., in the absence of aggregate), that is more prone to damage once crystalline sulfate attack reaction products begin to form in

the pores.

It is also to be emphasized that samples examined herein were small, unrestrained, and unreinforced cement pastes. The small size and lack of restraint or reinforcement was selected to accelerate the onset and progress of damage, as compared to concrete structures in practice.

1.3 *Influence of presence of aggregate*

In addition to examining neat cement pastes, sulfate-induced damage to Type I cement samples at w/c of 0.485 containing quartz aggregate particles were characterized by microCT. Figure 16 shows progressive damage to a sample containing aggregate after 7, 17, and 21 weeks of exposure, for comparison with a compositionally similar sample (without aggregate) in Figure 3. The aggregate are apparent as irregularly shaped inclusions, which appear in these 3D renderings like void space. The first appearance of physical damage in samples containing aggregate was in the form of edge cracks noted after 12 weeks of exposure. By 16 weeks exposure, cracks running along the length of the sample (longitudinal cracks) and body cracks were evident. By 17 weeks, extensive cracking and spalling at the edges and cracking within the sample body were evident, and further cracking and spalling was observed after 21 weeks exposure. The sample had completely disintegrated by 35 weeks.

For a detailed appreciation of damage evolution in these samples, microCT slices were examined (Fig. 17). While no damage was observed at 7 weeks of exposure, (Fig. 17(a)), at 17 weeks exposure (Fig. 17(b)) an interface crack partially surrounded aggregate particle AG1; body cracks BC1 and BC2 were present, with BC1 passing through the interface of cement paste matrix and aggregate particle AG3; radial cracks were also present. While no interface crack was observed around aggregate particle AG2 in this slice, a crack was present and linked to the surface at about slice number 60, i.e. closer to the end of the sample. A small amount of spalling was also observed. At 21 weeks exposure (Fig. 17(c)), the most notable change (compared to the matching slice at 17 weeks) was that aggregate particles AG1 and AG2 were completely outlined by interface cracks. The width of the interface crack at the position marked IC was 0.15 mm at 17 weeks and 0.23 mm at 21 weeks. Spalling was more severe and the radial cracks were more pronounced at 21 weeks than at 17 weeks. In addition, at 21 weeks of exposure, the linear attenuation coefficients of the cement paste matrix for area A1 near the sample surface (= 1.8 cm^{-1}) and region A3 near the sample core (=1.8 cm^{-1}) were less than the linear attenuation coefficients in the same regions at 7 (A1=2.7 cm^{-1}; A3=2.1 cm^{-1}) and 17 weeks of exposure (A1=2.4 cm^{-1}; A3=2.3 cm^{-1}). Regions A1 and A3 in the cement paste matrix were in close proximity to the aggregate, AG1, which by this exposure time was completely surrounded by an interface crack linked to the sample surface. Dissolution of the matrix material in the regions close to the interface crack likely led to decreases in density in regions A1 and A3, with linear attenuation coefficient of the aggregate particle AG1 confirmed to remain constant with time.

As compared to the corresponding cement paste sample (i.e., at w/c = 0.485 and exposed to 10,000 ppm of sulfate ions in a sodium sulfate solution), the progress of damage was more rapid in the cement paste-aggregate sample. Damage was first apparent by microCT in the sample containing aggregate at 12 weeks versus 17 weeks for the neat cement paste sample. At 17 weeks, damage in the cement paste-aggregate sample was much more extensive than in the absence of aggregate, as can be clearly seen comparing Figures 16 and 3. In the presence of aggregate, body cracks and radial cracks were much more often linked to interface cracks, indicating that the cement paste-aggregate interface facilitated more rapid progression of damage than in the aggregate-free samples. Notably, the cement paste sample remained intact beyond 78 weeks of exposure, while the cement paste-aggregate sample had completely disintegrated by 35 weeks.

Thus, as anticipated, the presence of aggregate appears to have accelerated both the initiation and progression of damage by sulfate attack. This is likely related to the increase in permeability associated with the cement paste/aggregate interface. Others have also suggested that the reaction of large calcium hydroxide crystals formed at the interface, during hydration, with ingressing sulfates to form gypsum (and, perhaps ettringite in the presence of aluminum) may also play a key role in the more rapid

degradation of cement-based materials containing aggregate [31]. Further EDXRD measurements, with particular attention to the aggregate/paste interface, are necessary to assess the relative importance of these potential reactions as compared to the inherent increase in permeability.

2.0 Conclusions

Results from an integrated sulfate research program which includes x-ray microtomography (microCT), energy dispersive x-ray diffraction (EDXRD), and measurements of strength and length change have been presented to examine the influence of cement type, water-to-cement ratio, and the presence of aggregate on sulfate resistance. All samples were exposed to 10,000 ppm sulfate in Na_2SO_4 solution. This research has produced results which support some commonly held understanding of the mechanisms of sulfate-induced damage in cement-based materials, while other observations do not fit with current understanding; key observations in both areas are highlighted below. One outcome of this research, then, is clearly the need for further fundamental research to link the chemical, physical, and mechanical changes occurring in cement-based materials during reaction with sulfate solutions.

Effect of cement type

Considering the expansion, strength, microCT, and EDXRD data, it is clear that cement composition has a strong influence on resistance to sulfate distress, with the Type V cement demonstrating greater resistance, as anticipated. That is, the Type V cement showed less expansion with exposure, no loss in compressive strength, later manifestations and slower progress of physical damage. These physical and mechanical differences are accompanied by chemical differences as seen by EDXRD including the observation that the shape of the ettringite depth profiles are distinct, with Type I showing more variation with depth. Another distinction with cement type is that at long sulfate exposure times gypsum is observed only in the Type V samples, where a band of gypsum is observed to "migrate" inward with continued exposure. The lower C_3A content, lower C_3S/C_2S, and higher C_4AF content are believed to be key factors influencing the improved resistance of Type V cement, as generally accepted.

Another interesting observation involves the relationships between the formation of gypsum and ettringite and the location of cracks, as detected by microCT, in a sample at 52 weeks of exposure. By EDXRD, an anticorrelation was observed between gypsum and ettringite. The data suggests that ettringite, with continuing sulfate exposure, has decomposed to form gypsum. With a crack detected very near the location in the paste where gypsum is formed, it is possible that a localized increase in sulfate ion concentration, due to localized increased permeability, may be a driving force for the formation of gypsum. However, the links between ettringite loss, gypsum formation, and cracking are not clear and should be examined further.

Effect of w/c

Under sodium sulfate attack, the onset and progression of physical deterioration (i.e., cracking, spalling, and disintegration) *in cement paste specimens* as detected by microCT occurred more rapidly at the *lower* w/c. These observations run counter to anticipated behavior and are not supported by measurements of expansion in mortar bar samples at the same two w/c values. For cement pastes, it was proposed that changes in extensibility and pore structure with decreasing w/c are likely factors contributing to the deterioration trends observed by microtomography.

Effect of aggregate

As anticipated, in the presence of aggregates a more rapid onset and progression of physical distress was observed. Damage was first apparent by microCT in samples with aggregate at 12 weeks sodium sulfate exposure, versus 17 weeks for the neat cement paste sample. Samples containing aggregate failed by 35 weeks exposure, while the corresponding cement paste samples had not completely disintegrated after 78 weeks exposure. In the presence

of aggregate, body cracks and radial cracks were often linked to cracks at the paste/aggregate interface.

References

1. P.K. Mehta, Sulfate attack on concrete- A critical review, in: J. Skalny (Ed.), Materials Science of Concrete III, American Ceramic Society, 1992, pp. 105-130.

2. K.E. Kurtis, P.J.M Monteiro, S. Madanat, Empirical Models to Predict Concrete Expansion Caused by Sulfate Attack, J. ACI Materials, 97 (2) (2000) 156-161. Errata, 97 (6) (2000) 713.

3. J. Skalny, J. Marchand, I. Odler, Sulfate Attack on Concrete, Spon Press, New York, 2002.

4. P.J.M. Monteiro, K.E. Kurtis, Time to Failure for Concrete Exposed to Severe Sulfate Attack Cem. Concr. Res., 33 (7) (2003) 987-993.

5. M. Santhanam, M.D. Cohen, J. and Olek, Sulfate attack research-whither now?, Cem. Concr. Res., 31 (6) (2001) 845-851.

6. W.G. Hime, B. Mather, B., Sulfate attack or is it?, Cem. Concr. Res., 29 (5) (1999) 789-791.

7. A. Xu, A. Shayan, P. Baburamani, Test methods for sulfate resistance of concrete and mechanism of sulfate attack, ARRB Transport Research, Review Report 5, 1998.

8. M.D. Cohen, B. Mather, Sulfate attack on concrete- research needs, ACI J. Materials, 88 (1) (1991) 62-69.

9. ASTM, Standard test method for length change of hydraulic-cement mortars exposed to a sulfate solution, ASTM Standard C1012 – 95a, Annual Book of ASTM Standards, (1996).

10. P.K. Mehta, Evaluation of sulfate-resisting cements by a new test method, J. ACI, 72 (1975) 573-575.

11. K.E. Kurtis, K. Shomglin, P.J.M. Monteiro, J. Harvey, J. Roesler, Accelerated tests for measuring resistance of calcium sulfoaluminate, calcium aluminate, and Portland cements, ASCE J. Mat. in Civil Eng., 13 (3) (2001)216-21.

12. American Concrete Institute (ACI), 201.2R-92: Guide to Durable Concrete, Farmington Hills, Michigan, 1992.

13. American Concrete Institute (ACI), 201.2R-01: Guide to Durable Concrete, Farmington Hills, Michigan, 2001.

14. S.R. Stock, N.N. Naik, A.P. Wilkinson, K.E. Kurtis, X-ray microtomography (microCT) of the progression of sulfate attack of cement paste, Cem. Concr. Res., 32 (10) (2002) 1673-5. Errata, 32 (12) (2002) 2002.

15. N. Naik, K. Kurtis, A. Wilkinson, A. Jupe, and S. Stock, Sulfate deterioration of cement-based materials examined by x-ray microtomography, Proc. SPIE 49th Annual Meeting, Optical Science and Technology: Developments in X-ray Tomography IV, Denver, August 2-6, 2004.

16. A.C. Jupe, S.R. Stock, P.L. Lee, N. Naik, K.E. Kurtis, A.P. Wilkinson, Phase Composition Depth Profiles using Spatially Resolved EDXRD, J. Applied Crystall., 37, (2004) 967-976.

17. I. Odler, I. Jawed, Expansive Reactions in Concrete, in: J. Skalny, S. Mindess (Eds.), Materials Science of Concrete II, American Ceramic Society, (1991) pp.221-47.

18. P.K. Mehta, personal communication with N.N. Naik.

19. Rasheeduzzafar, Influence of cement composition on concrete durability, J. ACI Mat., 89 (6), (1992), 574-586.

20. P.W. Brown, An evaluation of the sulfate resistance of cements in a controlled environment, Sulfate resistance of concrete, George Verbeck Symposium, ACI SP-77, (1982) pp. 83-91.

21. R.S. Gollop, R. S., H.F.W. Taylor, Microstructural and microanalytical studies of sulfate attack. I. Ordinary Portland cement paste, Cem. Concr. Res. 22 (6) (1992) 1027-1038.

22. R.S. Gollop, R. S., H.F.W. Taylor, Microstructural and microanalytical studies of sulfate attack. II. Sulfate-resisting Portland cement: Ferrite composition and hydration chemistry, Cem. Concr. Res., 24 (7) (1994) 1347-1358.

23. R.S. Gollop, R. S., H.F.W. Taylor, Microstructural and microanalytical studies of sulfate attack. III. Sulfate-resisting Portland cement: Reaction with sodium and magnesium sulfate solutions, Cem. Concr. Res. 25 (7) (1995) 1581-1590.

24. Rasheeduzzafar, O.S.B. Al-Almoudi, S.N. Abduljauwad, M. Maslehuddin, Magnesium-Sodium Sulfate Attack in Plain and Blended Cements, ASCE J. Mat, in Civil Eng., 6 (2) (1994) 201-222.

25. N.N. Naik, Sulfate attack on Portland cement-based materials: Mechanisms of damage and long-term performance, Ph.D. thesis, Georgia Institute of Technology, Atlanta, Georgia, 2003.

26. O. S. B. Al-Amoudi, Performance of fifteen reinforced concretes in magnesium-sodium sulphate environments, Const. Build. Mat. 9 (1) (1995) 25-33.

27. H. Haynes, Sulfate attack on concrete: Laboratory vs. field experience , Concr. International, 24 (7) (2002) 64-70.

28. C.J. Hampson and J.E. Bailey, The microstructure of the hydration products of tri-calcium aluminate in the presence of gypsum, J. Mat. Science, 18 (1983) 402-410.

29. P.K. Mehta, P.J.M. Monteiro, Concrete: Microstructure, Properties, and Materials, 2nd edition, Prentice-Hall, Englewood Cliffs, NJ, (1993).

30. G.W. Scherer, Crystallization in Pores, Cem. Concr. Res., 29 (8) (1999) 1347-58.

31. M.A. Gonzalez, E.F. Irassar, Ettringite formation in low C_3A Portland cement exposed to sodium sulfate solution, Cem. Concr. Res., 27 (7) (1997) 1061-1072.

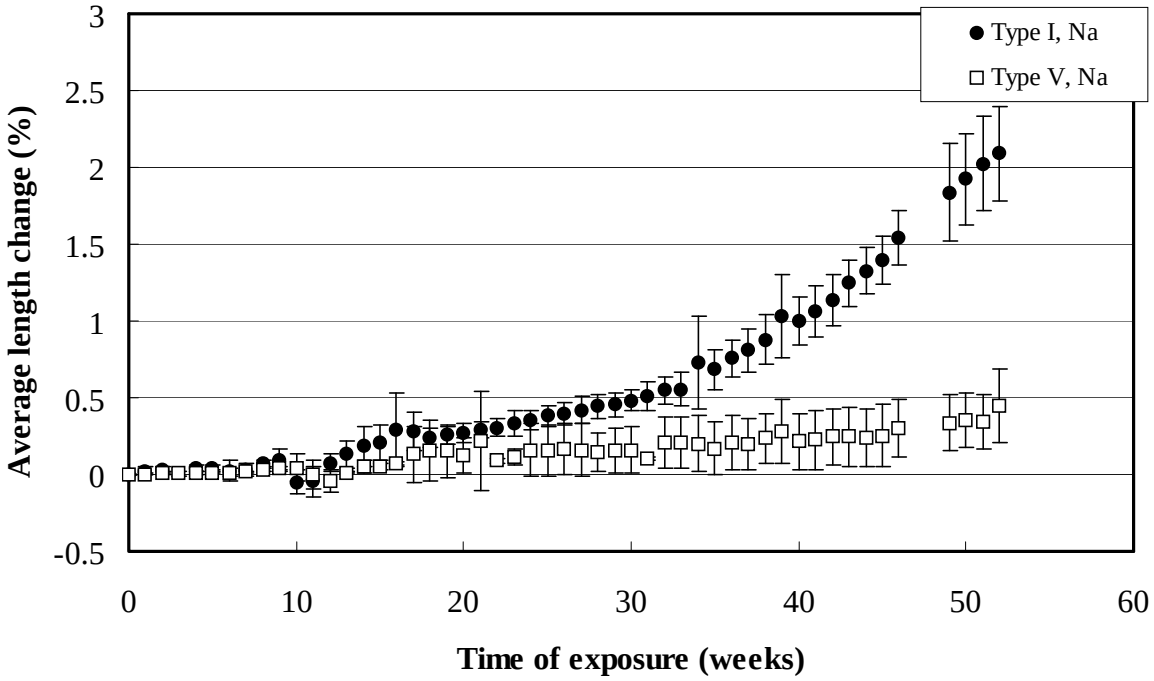

Fig. 1. Influence of cement composition on average expansion of mortar bars under sodium sulfate attack.

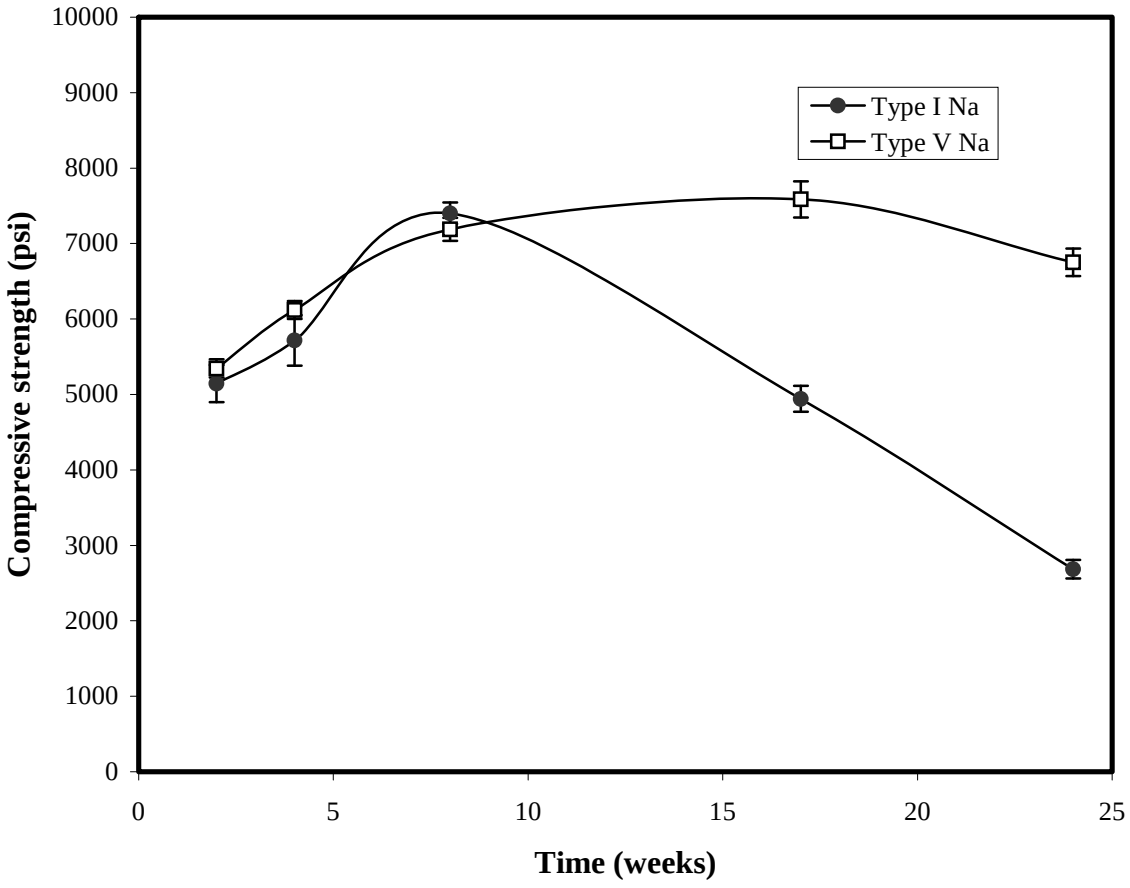

Fig. 2. Influence of cement composition on compressive strength with exposure to sulfate concentration of 10,000 ppm in sodium sulfate solution; trend lines shown as a guide to the eye.

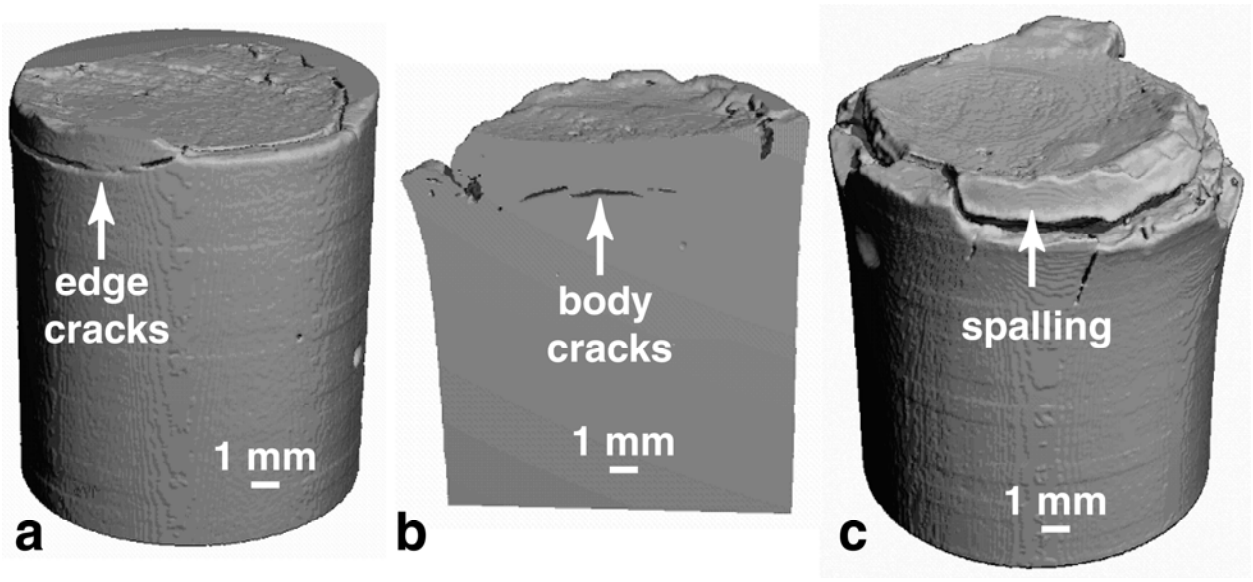

Fig. 3. Type I cement sample at w/c = 0.485 and exposed to sulfate concentration of 10,000 ppm in sodium sulfate solution showing: a) edge cracks at 17 weeks, b) spalling and body cracking at 42 weeks, and c) continued spalling at 52 weeks of exposure.

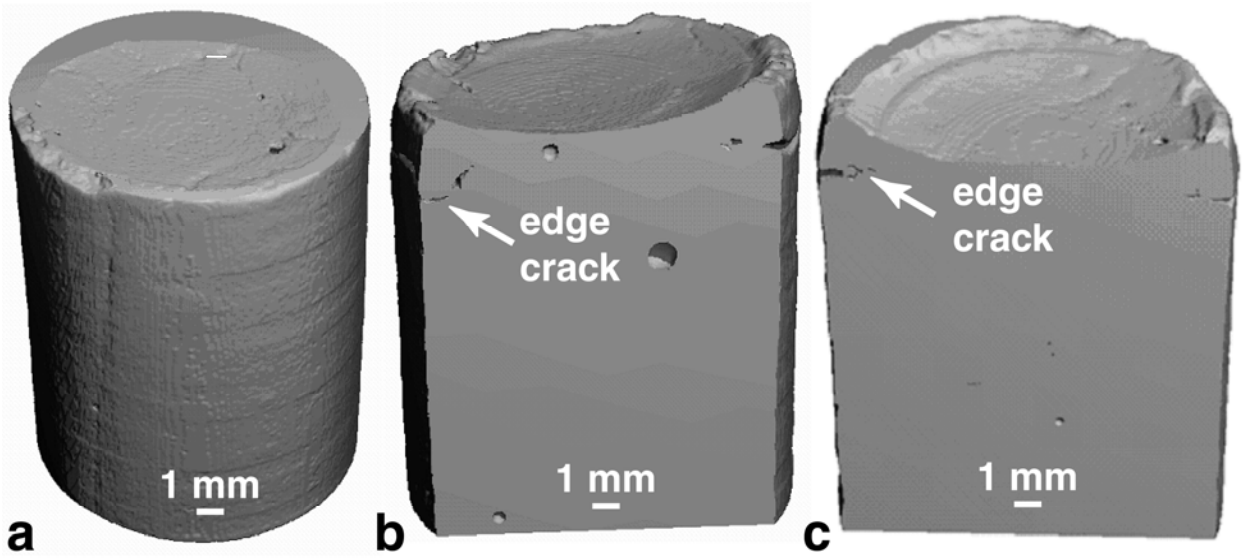

Fig. 4. Type V cement sample at w/c = 0.485 and exposed to sulfate concentration of 10,000 ppm in sodium sulfate solution showing: a) no damage at 17 weeks, b) edge cracking at 42 weeks, and c) continued edge cracking at 52 weeks of exposure.

a)

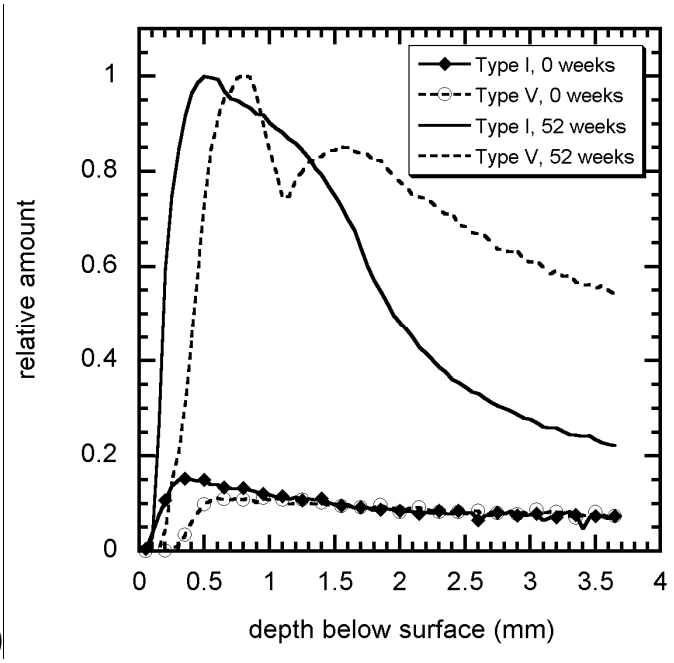
Type I, 0 weeks
Type V, 0 weeks
Type I, 52 weeks
Type V, 52 weeks
relative amount
depth below surface (mm)
0
0.2
0.4
0.6
0.8
1
0
0.5
1
1.5
2
2.5
3
3.5
4

b)

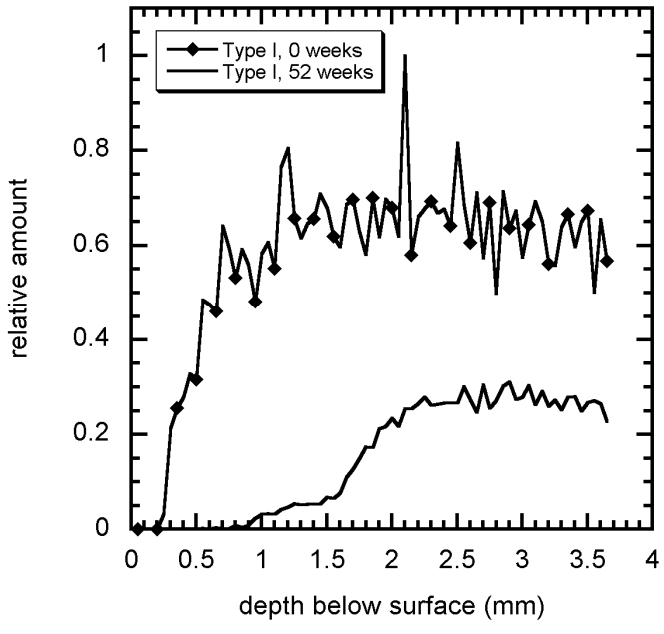
Type I, 0 weeks
Type I, 52 weeks
relative amount
depth below surface (mm)
0
0.2
0.4
0.6
0.8
1
0
0.5
1
1.5
2
2.5
3
3.5
4

c)

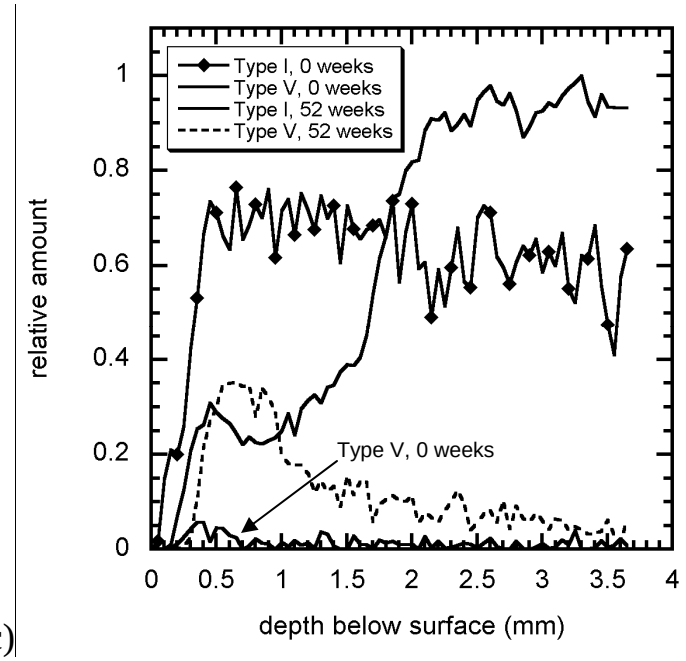

Fig. 5. Relative amounts of a) ettringite, b) monosulfate 12-hydrate and c) monosulfate 14-hydrate observed in specimens exposed to 10,000 ppm sulfate solution for 52 weeks are compared to those found in the corresponding controls. Within each panel, the plots are on the same relative scale enabling a quantitative comparison between the amounts of a given phase in different specimens.

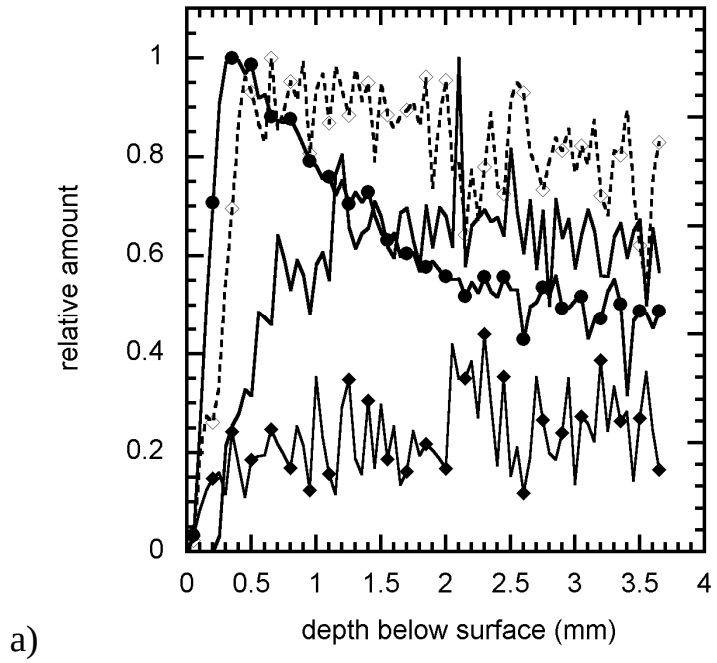

a)

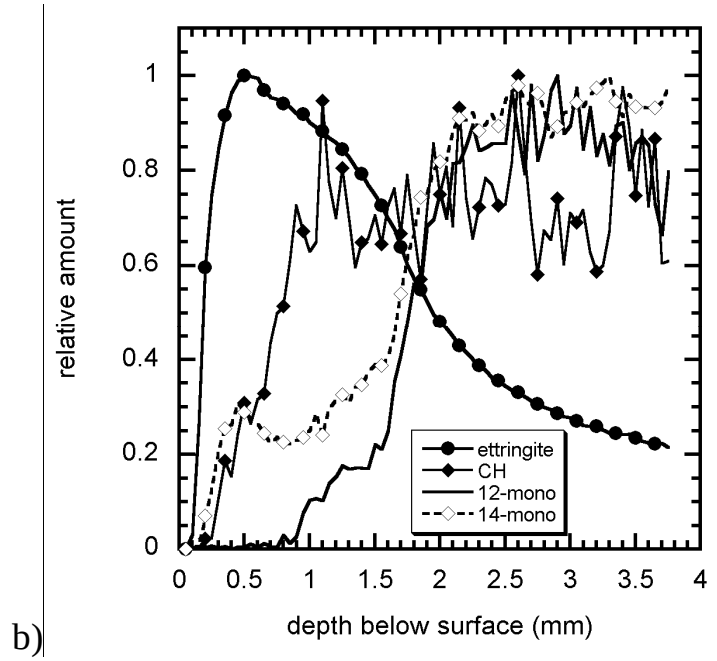

b)

Fig. 6. Composition depth profiles from EDXRD for Type I cement paste samples with w/c of 0.485 a) in control sample and b) in exposed sample after 52 weeks exposure to 10,000 ppm sulfate solution. The legend in 6(b) serves for both figures. As the scaling of the lines in the two panels has been chosen to best illustrate the spatial relationships between the various phases, it is not possible to quantitatively compare the amounts of the different phases within a panel or between panels.

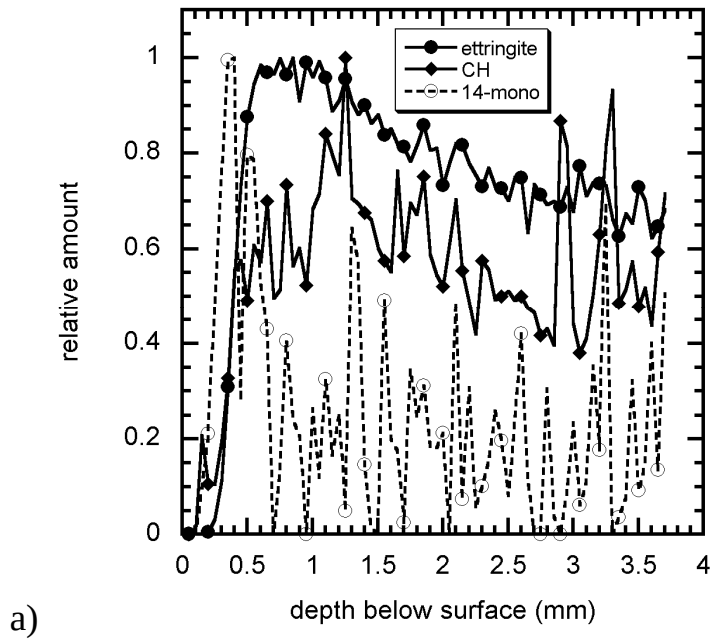

a)

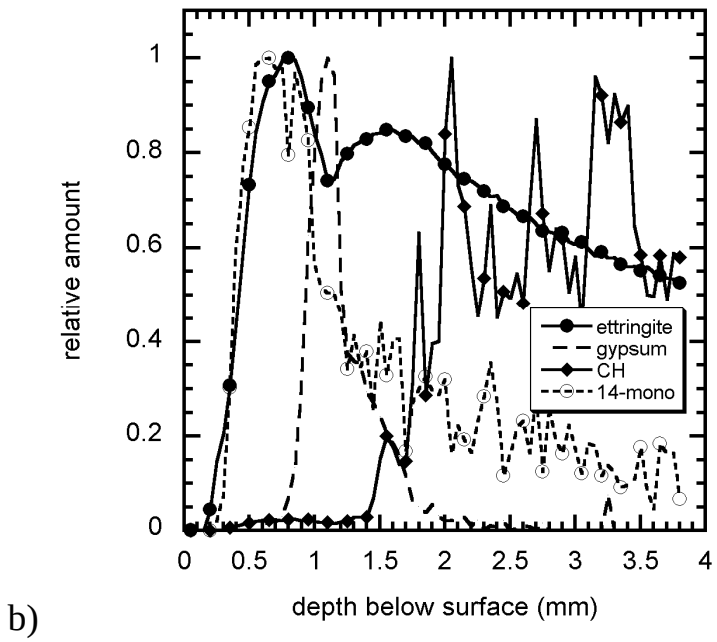

b)

Fig. 7. Composition depth profiles from EDXRD for Type V cement paste samples with w/c of 0.485 a) in control sample and b) in exposed sample after 52 weeks exposure to 10,000 ppm sulfate solution. As the scaling of the lines in the two panels has been chosen to best illustrate the spatial relationships between the various phases, it is not possible to quantitatively compare the amounts of the different phases within a panel or between panels.

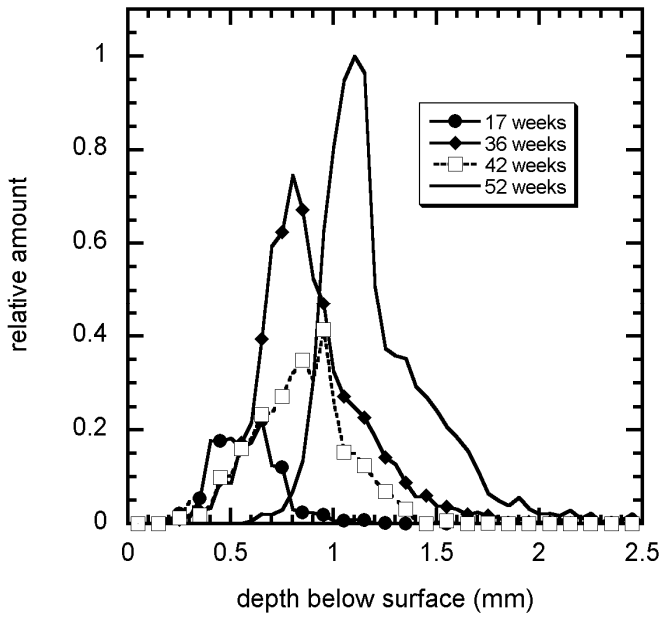

Fig.8. Gypsum concentration profiles as a function of sulfate exposure time as seen by EDXRD for a series of Type V cement paste samples with w/c of 0.485. All data are on the same relative scale permitting quantitative comparison.

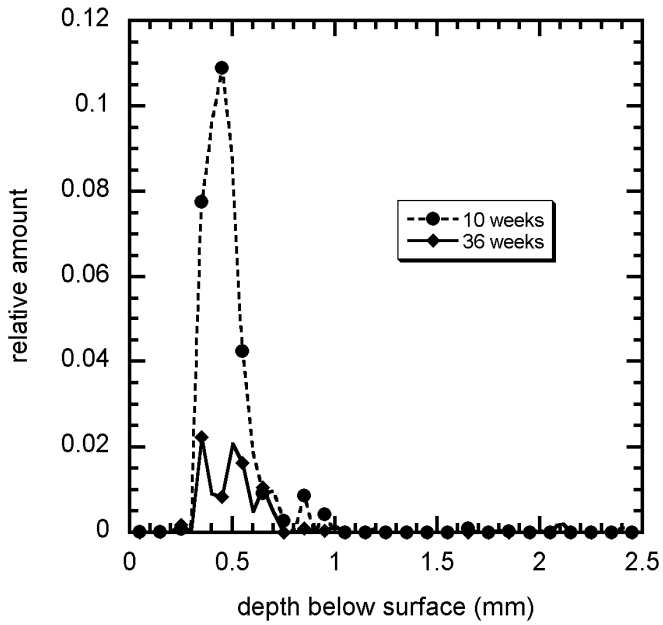

Fig.9. Gypsum concentration profiles as a function of sulfate exposure time as seen by EDXRD for a series of Type I cement samples with w/c of 0.485All data are on the same relative scale permitting quantitative comparison within this figure and with the data shown in Figure 8. No gypsum was detected in Type I samples exposed for longer than 36 weeks.

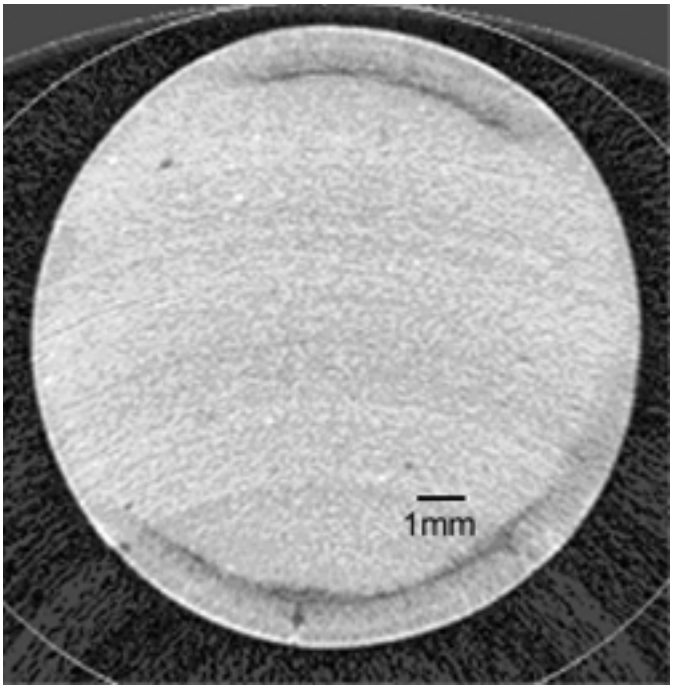

Fig. 10. Ring cracks are observed by microCT at ~0.9mm depth in Type V cement samples with w/c of 0.485 after 64 weeks exposure to sodium sulfate solution.

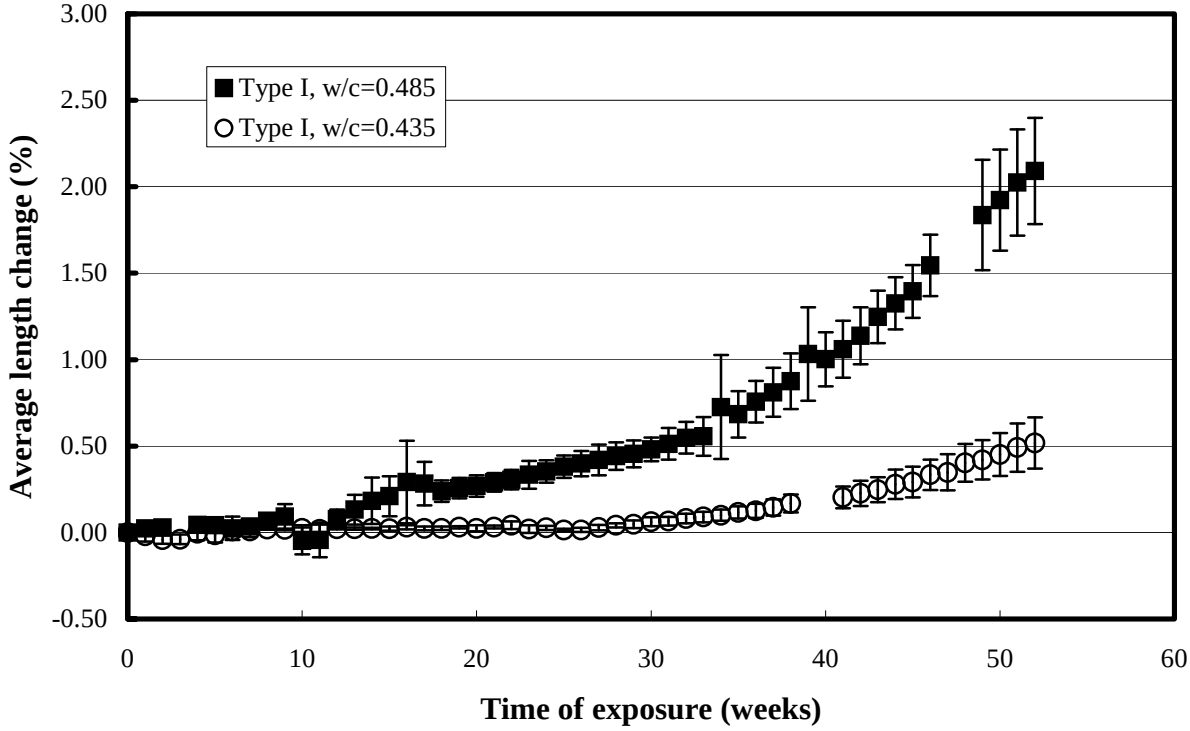

Fig. 11. Influence of w/c on average expansion of mortar bars under sodium sulfate attack.

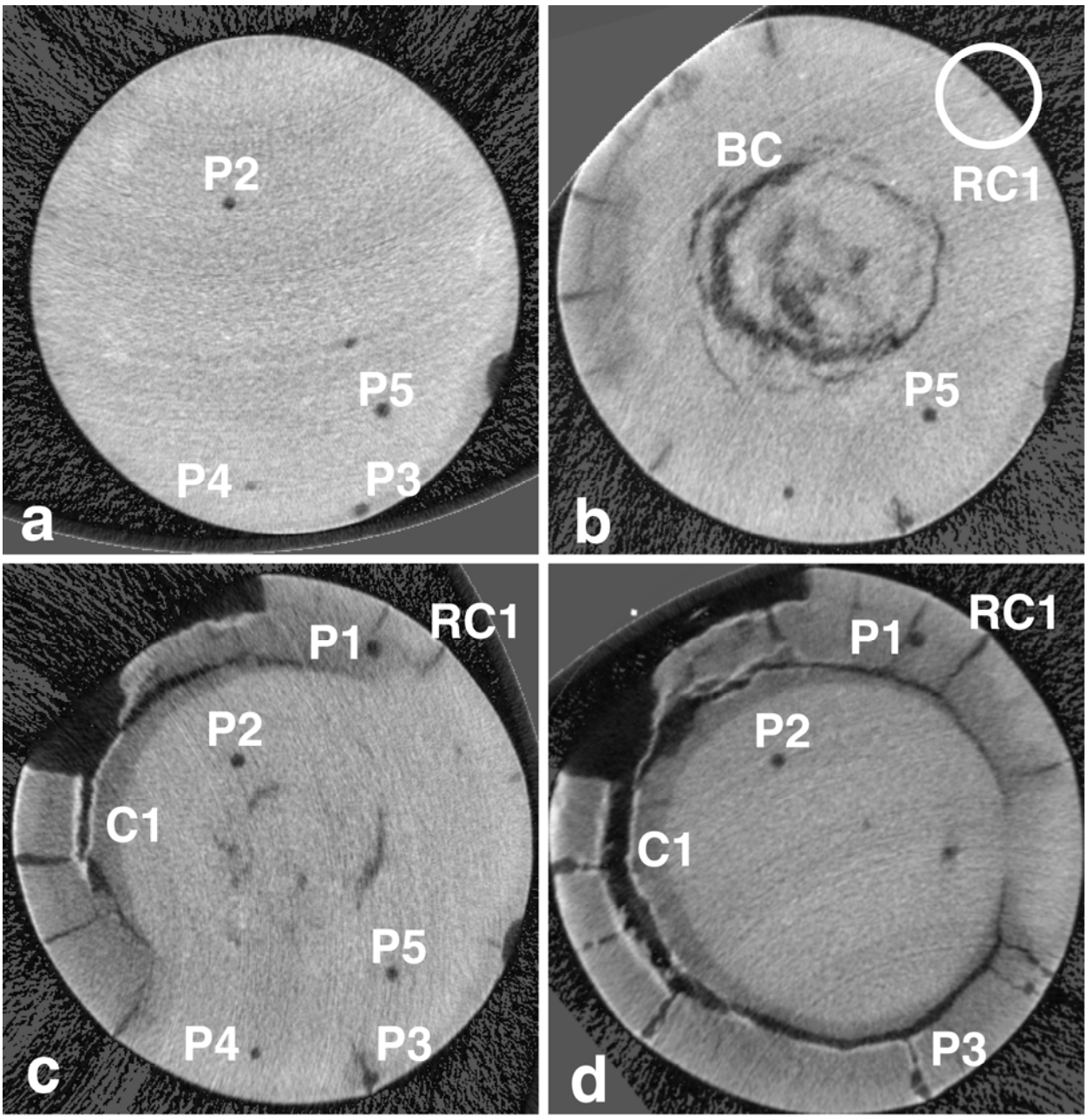

Fig. 12. Matching slices of a Type I cement paste sample at w/c of 0.485 and exposed to 10,000 ppm of sulfate ions in sodium sulfate solution after a) 21 weeks (slice number 70), b) 36 weeks (slice number 108), c) 42 weeks (slice number 71), and d) 52 weeks (slice number79), and showing crack C1, radial crack RC1, and pores P1-P5. The horizontal field of view is a) 15.3 mm, b) 15.1 mm, c) 16.1 mm, and d) 15.2 mm.

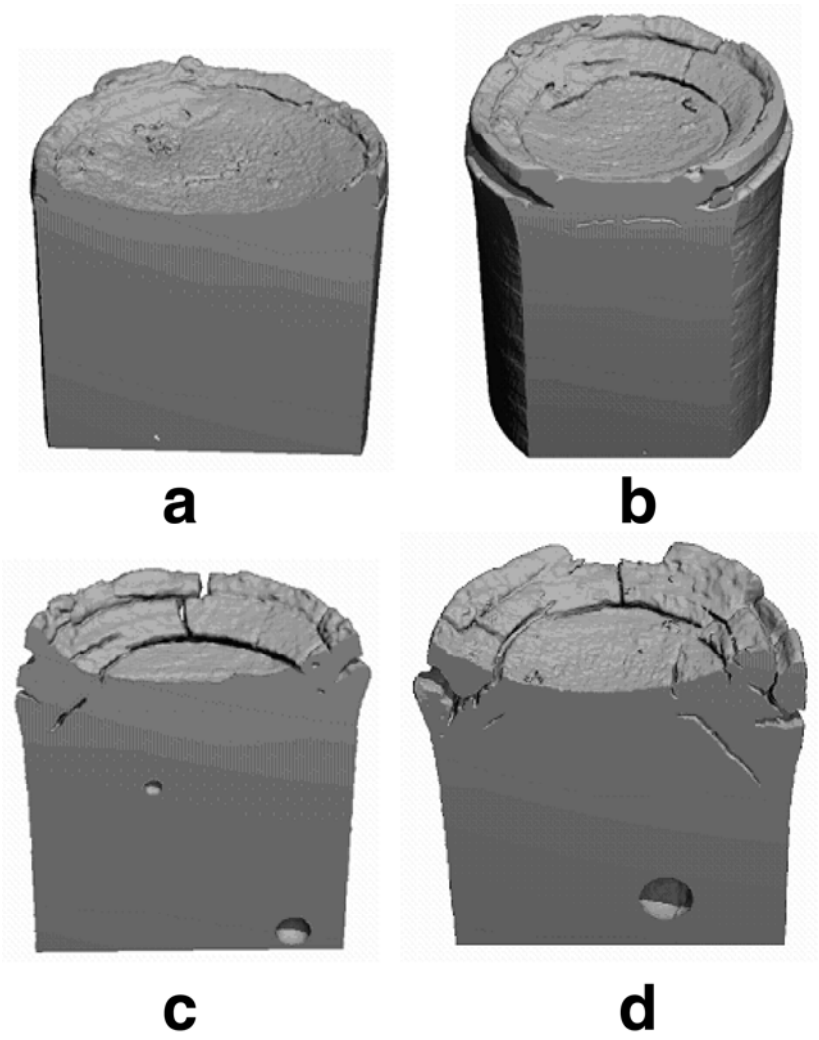

Fig. 13. 3D renderings of Type I cement paste sample at w/c of 0.435 and exposed to 10,000 ppm of sulfate ions in sodium sulfate solution for a) 9 weeks showing onset of cracking at the edges, b) 16 weeks showing widening of existing cracks and formation of new cracks, c) 22 weeks showing continued cracking, and d) 32 weeks showing increased cracking and spalling.

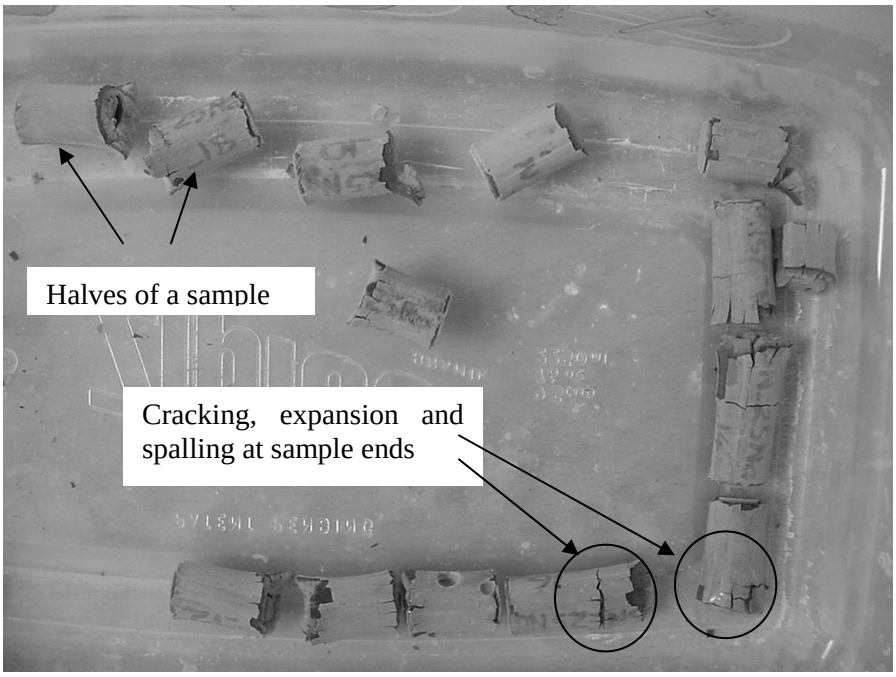

Fig. 14. Type I cement paste samples with w/c of 0.435 exhibited cracking and broke into halves at 56 weeks of exposure.

Fig. 15. Type I cement paste samples with w/c of 0.485 showed multiple cracks and some spalling at 108 weeks of exposure.

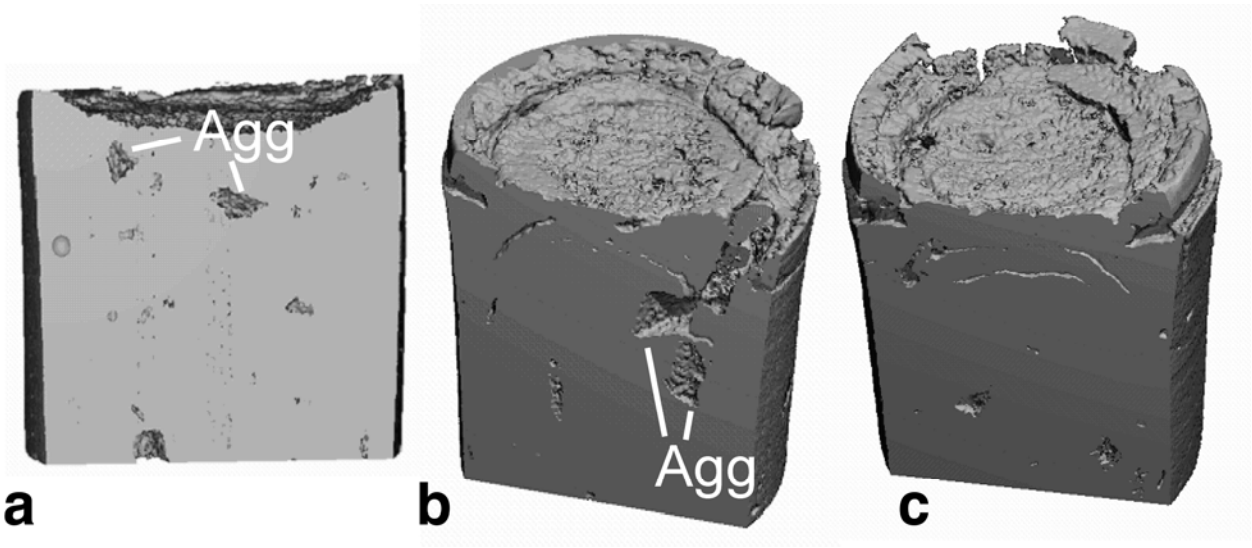

Fig. 16. Type I cement paste-aggregate sample at w/c of 0.485 and exposed to 10,000 ppm of sulfate ions in sodium sulfate solution for a) 7 weeks showing no damage, b) 17 weeks showing cracking and spalling at the edge and cracking within the sample body, and c) 21 weeks showing continued cracking and spalling.

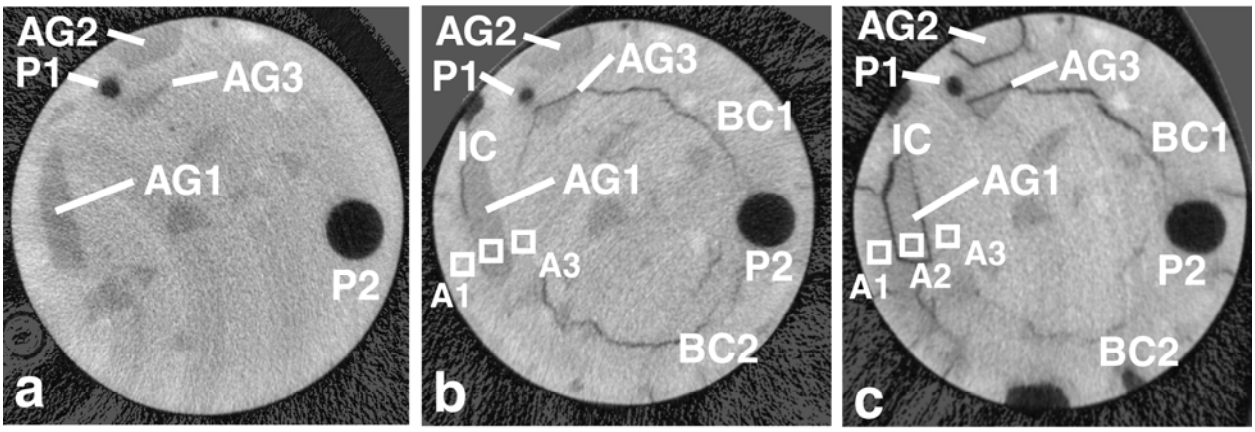

Fig. 17. Matching slice for Type I cement paste-aggregate sample at w/c of 0.485 and exposed to 10,000 ppm of sulfate ions in sodium sulfate solution for a) 7 weeks (slice number 88), b) 17 weeks (slice number 74), and c) 21 weeks (slice number 77), showing the presence of aggregate particles AG1-AG3, interface crack IC, body cracks BC1 and BC2, and pores P1 and P2. The horizontal field of view is a) 14.9 mm, b) 15.3 mm, and c) 16.8 mm.